Intermolecular Structure of Spherical Polyelectrolyte Microgels in Salt-Free Solution. 1. Quantification of the Attraction between Equally Charged Polyelectrolytes

Franziska Gröhn* and Markus Antonietti

Max Planck Institute of Colloids and Interfaces, D-14424 Potsdam/Golm, Germany

Received February 8, 2000; Revised Manuscript Received May 23, 2000

ABSTRACT: Static light scattering experiments were performed on spherical polyelectrolyte microgels in dilute aqueous solution. These particles realize a model system that is close to a "pure Coulombic" and "conformation-change free" polyelectrolyte. A more complete picture than in other studies is provided by the systematic examination of macroions over 1 decade of radii (6 nm < R < 70 nm), with its mesoscopic range of molecular mass for the first time covering the gap between linear polyelectrolytes and classical latex spheres. Solution structuring, phase-separation behavior, and concentration dependence of interparticle distances prove the presence of electrostatic attractive forces. This is confirmed by salt concentration and cross-linking-density-dependent experiments. Scattering data are also analyzed in the framework of Coulomb potential/MSA within the primitive model showing the existence of effective repulsive and attractive forces. On the basis of the experimental data, two qualitative pictures for the attraction mechanism are discussed: the "fluctuation model" and the "colloidal orbital approach".

1. Introduction

Interactions in systems of charged particles, flexible polyelectrolytes as well as charged colloidal particles, are still far from being understood.[1,2] The role of electrostatic repulsive and attractive forces was already discussed by Langmuir more than 60 years ago,[3] and this discussion has not lost its importance.

The interaction between colloidal particles is generally interpreted in terms of the well-established DLVO theory; i.e., the pairwise interaction potential is written as the sum of a repulsive screened Coulomb potential and an attractive van der Waals component. In this description, for highly charged colloids the far field contributions are purely repulsive. However, several experimental observations reported by different groups could not be explained by the classical DLVO model: in particular, interparticle distances smaller than expected for uniform particle distribution and the formation of void structures.[4−13] Over the past 25 years an enormous discussion about the nature of the pairwise interaction potential has arisen. Sogami and Ise were the first who proposed an alternative pairwise potential.[14] The validity of the Sogami−Ise theory is not discussed here; the reader is referred to the original literature or reviews.[15−24] It is just that this work broke the paradigm of the repulsion-only assumption. Meanwhile, there are more elaborated theories available that connect the electrostatic attraction of similarly charged objects with a molecular picture, e.g., by Belloni, who attributed the force to nonlinear counterion condensation which results in non-mean-field ion−ion correlations.[25,26]

Connected with the discussion about the nature of the interaction potential is likewise extended discussion about the corresponding experiments themselves. One reason is that the "classical" experiments by the Ise group, as well as more recent investigations by Grier and co-workers, refer to a two-dimensional layer of latex particles imaged by different microscopy techniques; thus, critics argue over wall effects.[27−32] On the other hand, phase separation effects in three-dimensional systems are ascribed to sedimentation effects.[33−36] Even after decades of discussion the results presented by different groups do not fit into a consistent picture.

Therefore, the study of interaction effects between charged colloids is still of interest, from the theoretical as well as the experimental point of view. A promising theoretical method based on multibody effects starting from basic thermodynamics and quantum mechanical analogy was recently presented by Schmitz.[37] From the experimental point of view, studies on well-defined model systems that avoid the bias of the previous systems are needed. In particular, experiments on optically transparent solutions of spherical polyelectrolytes are expected to be of advantage because the investigation of intermolecular interaction effects is not complicated by intramolecular conformation changes, as they are observed for linear flexible polyelectrolytes.

The disadvantages of polymer latex dispersions or silica spheres previously used as spherical model systems are twofold. First, these particles usually are relatively large as compared to linear polyelectrolytes. Therefore, particle-number-dependent effects are less marked, and problems with multiple scattering as well as sedimentation arise. Second, latex dispersions consist of dispersed particles with hydrophobic interiors; thus, additional dispersion forces might complicate the examination of electrostatic interactions. An ideal model system is expected to consist of small, purely hydrophilic, spherical particles.

At this point recent progress in polymer chemistry can be made use of, namely the polymerization in microemulsion leading to microgels: small polymer networks of well-defined mesoscopic size, low polydispersity, and highly perfect spherical shape.[38] These polymer microgels may be functionalized in a second step by polymer analogous reaction resulting in polyelectrolyte microgels of the same geometry.[39] Such polyelectrolyte microgels can be regarded as highly charged, spherical polyelectrolyte networks swollen in

10.1021/ma000235v CCC: $19.00
Published on Web 07/19/2000

aqueous solution. The species chosen in this study is poly(styrenesulfonic acid), showing a high degree of dissociation, which in addition is easily determined with a pH electrode. This model system has already been successfully applied in viscosity studies to prove the intermolecular origin of the polyelectrolyte effect.[39]

In this investigation, static light scattering experiments will be performed on dilute solutions of polyelectrolyte microgels with varying size, cross-linking density, polymer concentration, and added salt concentration. On the basis of these experiments, the presence of electrostatic attraction is quantified and discussed. Dynamic light scattering experiments on this model system will be presented in a future contribution.

2. Experimental Section

Polyelectrolyte Microgel Synthesis. The microemulsion polymerization technique has recently been reviewed[40] and is just briefly recapitulated. For the smaller particles with $R <$ 12 nm counterion modified surfactants such as cetyltrimethylammonium terephthalate and tartate[41] are used, whereas in other systems the cationic surfactants cetyltrimethylammonium chloride (CTMA) (for 12 nm $< R <$ 30 nm) and benzethonium chloride (for 30 nm $< R$) are used for microemulsification. Typically, 10 g of freshly distilled styrene, the estimated amount of cross-linker (e.g., 0.38 g of *m*-diisopropenylbenzene for a cross-linking density of 1/20 or one cross-link per 20 monomer units), and 50 mg of azobis(isobutyronitril) (AIBN) were mixed to form the oil phase. A solution of the calculated amount of surfactant (e.g., 20 g of CTMA, depending on the desired size of the microgel) in deionized water was prepared separately (100 g in total). Oil and water phases were mixed by vigorous stirring with a high-speed stirrer. After equilibrium is approached, the reaction mixtures were heated for 48 h at 60 °C. After this reaction time, the conversions exceeded 90% as estimated from the mass of the isolated polymer. The polymerized microlatex was dried in a vacuum at 50 °C and dissolved in THF and reprecipitated in methanol three times. The surfactants were completely removed by Soxhlet extraction with boiling methanol for 72 h, and the resulting microgels were dried in a vacuum at 50 °C.

Sulfonation of the styrene microgels was performed with H_2SO_4/Ac_2O in 1,2-dichloroethane at 55 °C.[39] The poly(styrenesulfonate) microgels precipitate from the reaction mixture when a degree of sulfonation of about 70% is reached (NMR analysis). The product is intensively washed with dichloroethane and cleaned by 3-fold dissolution in methanol and reprecipitation in diethyl ether and dried in a vacuum. With this procedure, the active ionic species is a poly(sulfonic acid), the advantage of which has been mentioned above. It is also stressed that this synthesis is ion- or salt-free; i.e., contrary to many other routes, the system is not afflicted with ionic impurities initially.

Since the "natural" polydispersity of a globular microemulsion is a Gaussian distribution of about 30% width, which is too broad for some of the present examinations, the samples were further fractionated by preparative ultracentrifugation. This was done by subsequent centrifugation of the aqueous polyelectrolyte microgel solution with increasing rotation speed from 5000 to 60 000 rpm (depending also on the initial size of the microgel). The gel-like sediment is redispersed in deionized water and kept as a final "fraction" whereas the supernatant is further fractionated. By this procedure each parental microgel sample is separated into about 8−10 fractions. Discarding the lowest and uppest fraction results in dust-free samples regarding high-density as well as low-density impurities.

For further investigations the samples were dissolved in deionized water, the solutions homogenized with a high-pressure homogenizer at 400 bar and stored over a mixed bed ion-exchange resin (Dowex MR-3, mixture of 1:1 HCR-S[H^+] and SBR[OH^-], 8% cross-linking, 20−50 mesh, Sigma Chemical Co.), thus resulting in salt-free solutions without aggregates. Polymer concentrations were checked by solid content and UV−vis spectroscopy after exposure to ion-exchange resin.

Table 1. Polymer Analytical Data of Polyelectrolyte Microgels Used in This Examination[a]

sample	ρ	r_H/nm (NaCl)	σ	M_w/g/mol
K5	1/20	77.2	0.15	245×10^6
K4	1/20	60.1	0.19	113×10^6
K73	1/20	55.0	0.11	82.2×10^6
K8	1/20	48.0	0.17	69.4×10^6
K24	1/20	43.5	0.05	46.8×10^6
K28	1/20	31.5	0.12	15.0×10^6
K33	1/20	23.7	0.12	8.30×10^6
K35b	1/20	19.8	0.14	5.40×10^6
K411b	1/20	6.7	0.11	*b*
K64	1/40	40	0.20	16.0×10^6
K2	1/80	38	0.24	13.8×10^6

[a] Given is the cross-linking density ρ as controlled by the ratio of mono- to bifunctional monomer during the synthesis, the hydrodynamic radius r_H(NaCl), and polydispersity σ as measured in 0.5 mol/L NaCl solution by dynamic light scattering as well as the molecular mass M_w estimated from the static light scattering data in 0.5 mol/L NaCl solution [b] Not measured.

Particle Size Characterization. The particle size and particle size distribution analysis is carried out at the different steps of the synthesis. Dynamic light scattering of the polymerized microemulsion in the initial dispersion is performed at a scattering angle of 90° (setup described below). The surfactant-free polystyrene microgels are characterized by angle-dependent static and dynamic light scattering in toluene. The final polyelectrolyte microgels are characterized in 0.5 mol/L NaCl solution by angle-dependent static and dynamic light scattering as well as analytical ultracentrifugation (Beckman Optima XL-I analytical ultracentrifuge).

The samples for further investigation are chosen on the basis of the distribution width obtained from analytical ultracentrifugation. Hydrodynamic radii measured by dynamic light scattering in 0.5 mol/L NaCl, an interaction-poor state, are used as reference radii in the following discussion. In Table 1 hydrodynamic radii are given as well as the width of their distribution as standard deviation of a Gaussian distribution. Also shown are the molecular weight data obtained from static light scattering.

Light Scattering Measurements. Light scattering measurements were performed with a setup for combined static and dynamic light scattering consisting of an ALV/SP-86 goniometer and an ALV-5000/E multitau correlator. A frequency-doubled Nd:YAG laser (Coherent/Adlas DPY 425 II) operating at a wavelength of 532 nm with a maximum output power of 400 mW was used as light source. Measurements were performed at scattering angles of 15°−150° (usually in 1° steps from 15° to 50° and in 2.5° steps from 50° to 150° for scattering curves and in 5° steps for molecular weights). The volume corrected scattering intensity of the toluene standard lies within ±2% statistical error. All scattering intensities are corrected by solvent subtraction.

The time autocorrelation function of the scattered intensity was measured (homodyne mode) and converted to the scattered electric field autocorrelation function via Siegert relation. The electric field autocorrelation function is analyzed via inverse Laplace transformation using the program CONTIN by S. Provencher. The apparent diffusion coefficient was calculated from the inverse relaxation time via the Landau−Plazcek relationship and extrapolated to zero scattering vector. Hydrodynamic radii are obtained via the Stokes−Einstein relation from the extrapolated diffusion coefficients.

The solutions were cleared of dust particles by filtering through a Millipore 0.45 μm pore size cellulose nitrate filter into 1 cm diameter dust-free quartz cells which were coated with the solution itself prior to use, thus avoiding concentration changes by adsorption of the macroions onto the cell surface. The cell also contains some dust-free mixed bed ion-exchange resin at the bottom.

3. Results and Discussion

Spherical polyelectrolyte microgels were synthesized via polymerization in microemulsion, with subsequent polymer analogous reaction and (in contrast to earlier works) final fractionation by preparative ultracentrifugation. The molecular properties of some microgels are summarized in Table 1. The size range of 6 nm < R < 70 nm (for the swollen microgels) is covered for a cross-linking density of 1/20 chosen as reference state. For one fixed size also particles with cross-linking densities 1/40 and 1/80; i.e., more loosely cross-linked microgels have been synthesized.

Comparison of the molecular data prior to and after polymer analogous sulfonation shows that the functionalization takes place without changing the architecture. The observed molecular weight increase corresponds well with a mass increase due to 70% sulfonation. The swollen 1/20 cross-linked polyelectrolyte microgels in 0.5 mol/L NaCl solution are only slightly larger than the corresponding parental polystyrene microgels in toluene. (The direct comparison which can be made for the nonfractionated samples is very useful for that purpose.) It is stressed again that the described three-step synthesis yields narrowly distributed (5% polydispersity) small (down to 6 nm) and clean polyelectrolyte microgels.

Experiments were carried out with the poly(styrenesulfonic acid) with the protons as counterions, which not only show a high counterion activity but also can be kept salt-free during the measurement easily by adding ion-exchange resin.

It has to be noted that the radius of the polyelectrolyte microgels in solution is 1.5 times the one of the dispersion due to the swelling with solvent. This is in contrast to classical latex dispersions, but one of the strength of the present model system. The volume increase means that the inside of the microgel consists of a "25% polymer solution"; i.e., the ionic strength inside causes an intramolecular screening of electrostatic effects. This enables the dissociation of protons from a flexible, spherical object without pronounced hydrophobic effects or internal structure changes. Furthermore, swelling of the core diminishes the classical van der Waals attraction between the particles, which are typically strong for latex dispersions and overlap with the Coulomb interactions. Therefore, we consider our system as a close-to-pure Coulombic (or van der Waals poor) colloidal model system.

A. Concentration Dependence in Salt-Free Solution. Figure 1 displays scattering curves of the sample with R = 48 nm (cross-linking density 1/20) for salt free solutions with polymer concentrations between 1×10^{-3} and 1 g/L, corresponding to volume fractions between 1×10^{-5} and 1×10^{-2}. It is seen that the scattering curves show a pronounced first maximum plus up to three higher order peaks, indicating a relatively long-ranged ordering of the particles.

For discussion, the measured scattering intensity $I(q)$ has to be separated into the form factor $P(q)$ and the intermolecular structure factor $S(q)$. Since in the model system examined here the particle geometry is fixed and known to be spherical, this separation is not afflicted with any of the problems occurring in the case of linear flexible polyelectrolytes. For monodisperse spheres, the scattering intensity is given via

$$I(q) = bP(q)\,S(q) \qquad (1)$$

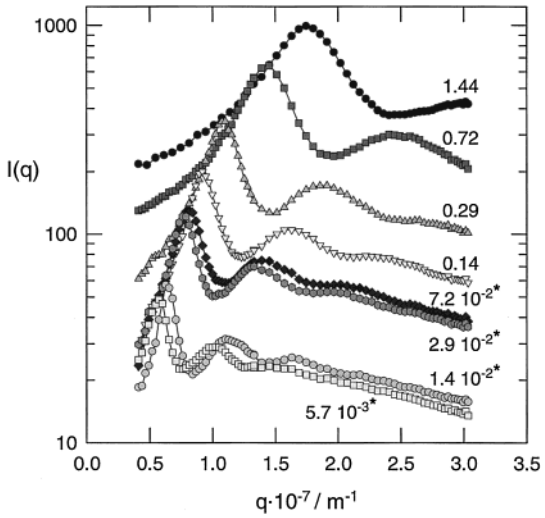

Figure 1. Scattering curves for polyelectrolyte microgel K8 with r_H = 48 nm in salt-free solution at different polymer concentrations, given in g/L. For phase-separated samples the scattering curves of the polymer-rich phase are shown (marked with an asterisk).

with the concentration-dependent constant b. The sphere form factor $P(q)$ is given by the well-known relationship

$$P(q) = \left[\frac{3\sin(qR) - 3(qR)\cos(qR)}{(qR)^3}\right]^2 \qquad (2)$$

We have applied two different methods to separate $I(q)$ into $P(q)$ and $S(q)$. In one approach, the sphere form factor is extracted from the scattering curve by fitting the high-q part, where structure influence is low, with a monodisperse sphere form factor according to eq 2. A representative example together with the resulting intermolecular structure factor is shown in Figure 2. Alternatively, the whole scattering curve can be inverted into real space as far as possible as a "polydisperse sphere form factor", according to

$$P(q) = \int_0^\infty D(R)\,P_0(q,R)\,\mathrm{d}R \qquad (3)$$

Using sphere form factors $P_0(q)$ as in eq 2 as basis functions and applying a regularized least-squares procedure[42,43] allows for the extraction of the form factor (and thereby an approximated size distribution $D(R)$) from the scattering curve. The resulting structure factors obtained via both methods are approximately the same. Here, we already take profit of the small particle sizes of our system, which—contrary to classical latex particles—possesses only a weakly angular dependent form factor without any oscillations in the q range of light scattering and thereby provides an easy-to-separate structure factor. It should be noted that by this procedure we do not quantitatively rely on the particle size measured in 0.5 mol/L NaCl solution, or any assumption about the amount of swelling, but determine the form factor in the salt-free solution itself. Further, we do not observe any relevant change in the form factor with polymer concentration.

The resulting structure factors show first maxima between 1.5 and 3.0 and relative peak positions of 1: 1.7: 2.6: 3.4. Renormalization of the structure factors (corresponding to the scattering curves of Figure 1) by the position of the first maximum results in the congruent curves shown in Figure 3. The result indicates that

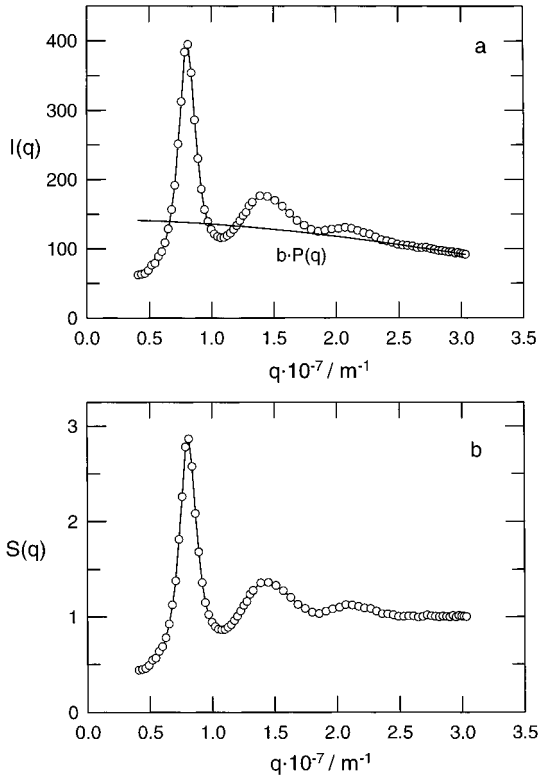

Figure 2. (a) Measured scattering intensity $I(q)$ for a polyelectrolyte microgel with $r_H = 43.5$ nm (symbols) and sphere form factor $bP(q)$, as obtained by a fit to the high q data points (full line). (b) Interparticle structure factor $S(q)$ as obtained from (a).

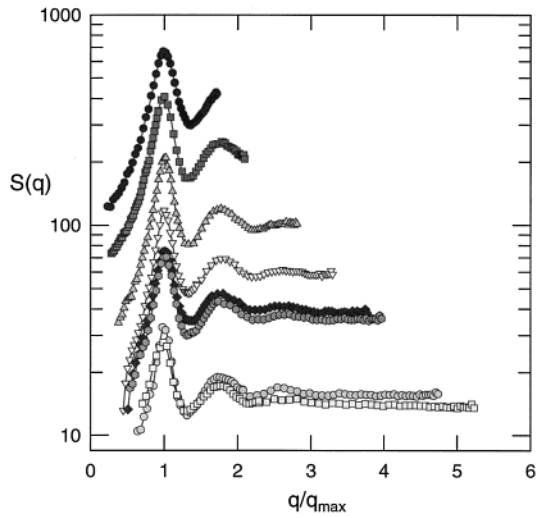

Figure 3. In the q axis normalized structure factors for the scattering curves shown in Figure 1. The data are normalized to a relative first peak position of one. The structure is the same for all investigated concentrations, only on a different scale.

merely the scale, but not the kind of structure, changes with concentration. Therefore, it is allowed to use the q value of the first maximum in the structure factor for studying concentration dependencies. The first peak position gives the interparticle distance. In a simplified view, the value

$$d_{exp} = \sqrt{\frac{3}{2}}\frac{2\pi}{q_{max}} \tag{4}$$

can be seen as the average nearest-neighbor distance

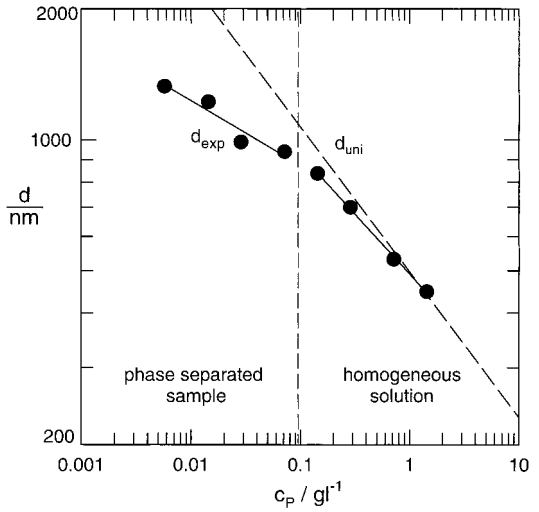

Figure 4. Interparticle distance obtained from the peak position in $S(q)$ as a function of the polymer mass concentration for the polyelectrolyte microgel with $r_H = 48$ nm in salt-free solution. The line shows the calculated distance for an ideal solution of uniform distributed particles: The experimental interparticle distance is significantly lower than that expected for uniform distribution and also shows a different scaling behavior.

Table 2. Solution Parameters and Interparticle Distance Data for Concentration-Dependent Experiments on Polyelectrolyte Microgel K8 with r_H(NaCl) = 48 nm in Salt-Free Solution[a]

c_P/(g/L)	N_P/L^{-1}	ϕ	d_{exp}/nm	d_{uni}/nm
1.437	1.25×10^{16}	5.78×10^{-3}	431.0	431.2
0.718	6.24×10^{15}	2.89×10^{-3}	530.7	543.3
0.287	2.49×10^{15}	1.16×10^{-3}	712.5	737.3
0.144	1.25×10^{15}	5.78×10^{-4}	836.4	929.1
0.072	6.24×10^{14}	2.89×10^{-4}	955.9	1170.3
0.029	2.49×10^{14}	1.15×10^{-4}	1005.9	1589.4
0.014	1.25×10^{14}	5.79×10^{-5}	1202.4	2000.3
5.74×10^{-3}	4.98×10^{13}	2.31×10^{-5}	1326.7	2717.9

[a] Given are polymer mass concentrations c_P, as well as particle number densities N_p and volume fractions ϕ as estimated from the independently determined polymer analytical data in Table 1. d_{exp} is the experimental interparticle distance as obtained from the structure factor peak maximum via $d_{exp} = (3/2)^{0.5}2\pi/q_{max}$, and d_{uni} is the theoretical distance for uniform distribution.

between the particles (exact value for a cubic lattice). Figure 4 shows this interparticle distance as a function of the polymer mass concentration, again exemplarily for the polyelectrolyte microgel with $r_H = 48$ nm, along with the "theoretical" interparticle distance d_{uni} calculated for uniformly distributed particles via

$$d_{uni} = \frac{1}{N_p^{1/3}} \tag{5}$$

with

$$N_p = \frac{c_P N_a}{M_w} \tag{6}$$

It has to be noted that the interparticle distances lie between 200 and 2000 nm, i.e., are much larger than the particle dimensions. Data are also given in Table 2.

Considering the right part of Figure 4, one finds a scaling of the interparticle distance with polymer mass concentration of $c_P^{-0.25}$. This is significantly different from the $c_P^{-0.33}$ scaling expected for uniform particle

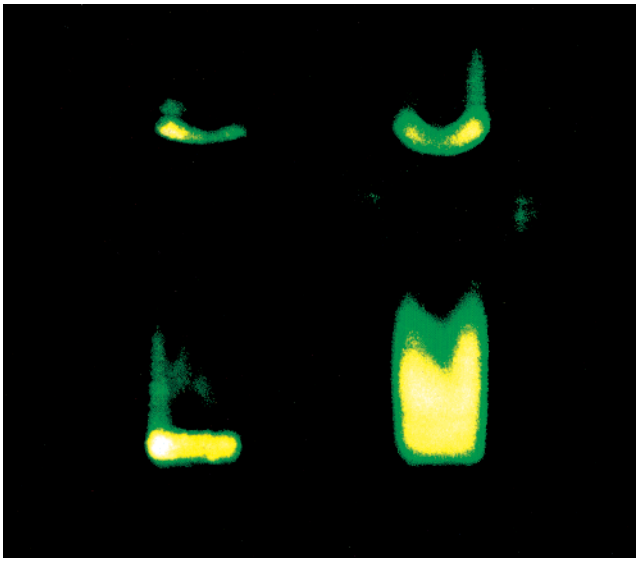

Figure 5. Photos of two phase-separated samples for the polyelectrolyte microgel K8 with $r_H = 48$ nm in salt-free solution with initial polymer concentrations of 7.5×10^{-3} g/L (left) and 7.5×10^{-2} g/L (right) under 90° laser illumination. Two phases with different scattering power are seen. With decreasing initial polymer concentration the volume of the polymer-rich phase decreases.

distributions. By comparing the experimental and theoretical data, it is clearly seen that the experimental interparticle distance is significantly lower than the one estimated for uniform distribution.[44]

The different scaling behavior and the interparticle distances smaller than expected for uniform distribution already demonstrate the existence of "electrostatic attraction" and point to a coexistence of structured regions with higher particle density and regions with lower particle density ("voids").

When the concentration is lowered below a certain value, 0.1 g/L in this case, solutions undergo a macroscopic phase separation. The interparticle distances of the polymer-rich phase are plotted as a function of the initial polymer mass concentration in the left part of Figure 4. A clear change in slope is found at the phase separation concentration. For the polymer-rich phase of the separated samples, the interparticle distance shows only a slight increase with decreasing initial polymer concentration.

A more precise picture of the macroscopically phase-separated samples has to be given. While a uniform colorless solution is seen by naked eye, two phases with different scattering power are observed in laser light: a lower phase with high scattering intensity and an upper phase with lower scattering intensity. Scanning of the scattering power through the sample shows a relatively sharp increase at a specific height of the cell to about 200-fold intensity. Photos of two phase-separated samples with different initial concentrations taken under 90° laser illumination are shown in Figure 5. The right picture is of the "first" phase-separated sample. The ratio of macroion regime to that of the void region seems to be unity, which corresponds very well to a void content of 0.5, as estimated from the reduction of interparticle distances for the "last" homogeneous sample (with the lowest concentration). With further decreasing the initial particle concentration, the relative content of the polymer-rich phase further decreases as seen in the example left in the figure.

Further, the scattering curves itself were measured in dependence of the height. The lower phase shows scattering profiles with well-defined peaks that were already shown in Figures 1 and 3 (marked with an asterisk). No pronounced angular dependent scattering is found in the upper phase, i.e., no structuring. Because of the low scattering intensity of this phase (1/200 of the polymer-rich phase), it was not reasonable to quantitatively analyze data from the upper phase. More importantly, we find that within the lower phase the scattering curves appear to be independent of the height. The position of the first maximum is the same; i.e., the interparticle distance is constant throughout this phase. The constant interparticle distance within the lower phase strictly excludes sedimentation as a possible reason for the phase separation. Phase separation is only due to thermodynamic reasons and must originate from interparticular forces. This topic will be discussed in section F.

It is also noted that our experimental set strongly supports recent data by Harada and Matsuoka et al., who examined the electrostatic attraction of classical colloidal disperisons by USAXS and report interparticle distances that are smaller than for uniform distribution in dependence of salt concentration.[45−47] Since they discuss their data in terms of κR (κ inverse Debye screening length, R particle radius), we briefly address this parameter for our system: The screening length $1/\kappa$, as determined by the concentration of the dissociated counterions, can be easily estimated via the pH of the solution (one advantage of the applied acidic model system). In fact, the solutions investigated in this study cover a range from $\kappa R \approx 0.05$ to $\kappa R \approx 5$; i.e., the Debye length is (partly) in the same order of magnitude as the particle size, as for the samples investigated in refs 45−47. However, in contrast to their study, interparticle distances usually are larger than the Debye lengths for our system (interparticle distances of 200−2000 nm for Debye lengths of 15−750 nm).

Considering relevant length scales, it should be further mentioned that the parameter space covered within this study also ensures the condition that the interparticle spacing calculated for uniform distribution is much larger than a likely location of a minimum in interaction energy, as was recently demanded by Schmitz.[18] This is in contrast to several other studies, which "prove" the accuracy of the DLVO potential within a distance range where any interaction potential in discussion would be repulsive anyway, as is also discussed in ref 18. Because of the high counterion activity, for our poly(styrenesulfonic acid) microgels, these distance conditions can be realized even for salt-free solutions. Therefore, it is possible to observe "electrostatic attraction" via particle distances and phase behavior quite obviously.

B. Data Analysis in Terms of the MSA/Primitive Model. A common way of handling data on systems of charged macroions is the mean spherical approximation (MSA) in combination with the screened Coulomb potential via the Ornstein−Zernicke equation. From our point of view it seems to be didactically useful to apply the primitive model in which macroions as well as small ions are considered via the Ornstein−Zernicke equation, i.e.

$$h(r) = g(r) - 1 = c(r) + \rho \int c(|\mathbf{r} - \mathbf{r}'|) h(r')\, \mathrm{d}\mathbf{r}'$$

with

$$g_{ij} = 0 \qquad \text{for } r < 2R$$

$$c_{ij} = \frac{V(r)}{kT} \quad \text{with } V(r) = \frac{z_i z_j e^2}{4\pi\epsilon_r\epsilon_0 r} \qquad \text{for } r > 2R \quad (7)$$

In this section we apply a refined version described by Blum and Hoye.[48−50] These authors developed an expression for the Laplace transform of the pair correlation function which consists of three terms: a Percus−Yevick hard-sphere contribution, an excess electrostatic contribution, and a third term resulting from charge-hard-core cross-contributions which can be neglected for small concentrations. For details the reader is referred to the original article or discussions of other authors.[51,52] In this work, we slightly modified the Blum−Hoye method by directly calculating the Fourier transform of the pair correlation function, i.e., the structure factor. The scattering curve is described within this model by fitting the parameters "*hard-core radius*" R and "*polydispersity*" σ (form factor), "*MSA radius*" R_{RMSA}, and "*charge*" z (structure factor) via nonlinear least-squares method. The resulting fitted structure factor can be Fourier transformed into the pair correlation function $g(r)$,

$$S(\mathbf{q}) = 1 + \rho\int \exp(-i\mathbf{qr})[g(\mathbf{r}) - 1]\, d\mathbf{r} \quad (8)$$

which again is converted to the "*potential of mean force*" $V(r)$ via a simple Boltzmann relation

$$g(r) = \exp\left(\frac{-V(r)}{kT}\right) \quad (9)$$

Figure 6 shows an example for obtained $g(r)$ and $V(r)$ curves. For the sample with R = 48 nm, the fit parameters are $\sigma = 0.1$, $R_{RMSA} = 347$ nm, and $z = 56 \times 10^3$. As seen in Figure 6a, estimates via this very simple formalism for the pair potential provide adequate results in terms of the structure factor features. As expected, it also yields extremely high values for *MSA radius* and *charge*. This is the well-known limitation to non-rescaled MSA and has been intensively discussed. Pair correlation function $g(r)$ and mean force potential $V(r)$ in parts c and d of Figure 6, respectively, show regions of effective repulsion as well as attraction. However, the description of the scattering curve (Figure 6a) is within a degree of accuracy which does not exclude the assumption of other interaction potentials as presented by different authors.[53−59] In all these cases the structure factor is equally well fitted, which allows the presented model to be called consistent with the experiment, but this does not necessarily exclude other models. The structure factor alone is not sensitive enough to distinguish between different pair potentials.

Therefore, the proof of attraction cannot rely on the shape of the scattering curve, but additional experimental results have to be considered. One is the microscopic or macroscopic phase separation described above which obviously cannot be explained within the model of Coulomb potential/MSA. All MSA approaches (*primitive model* as well as *one component macrofluid*, i.e., with or without explicitly regarding the counterions) lead to scaling exponents of $^1/_3$, as discussed in ref 60. Another weakness of any "mean-spherical" model is that obviously no effects of anisometric particle ordering are considered, a point that will be discussed in section F.

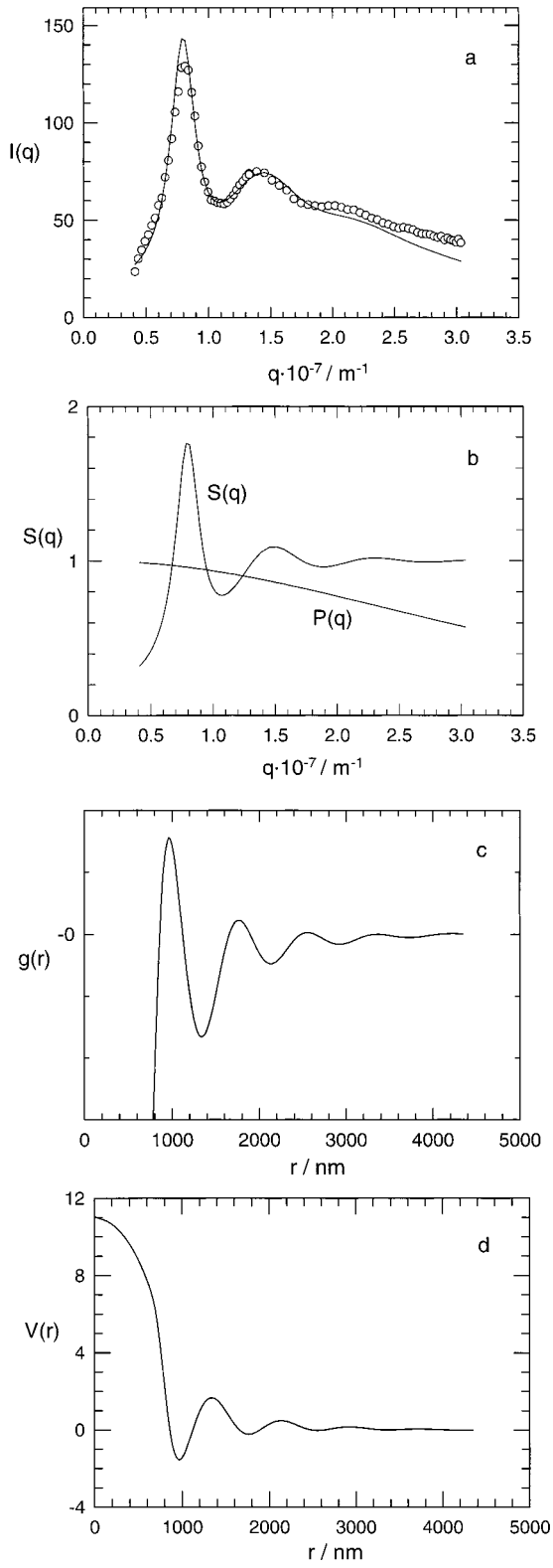

Figure 6. Data analysis in terms of MSA/Coulomb potential within the primitive model: (a) experimental scattering curve (circles) and fit (line), (b) structure factor $S(q)$ and form factor $P(q)$, (c) pair distribution function $g(r)$ (arbitrary units), (d) potential of mean force $V(r)$ (arbitrary units), showing regions of effective repulsion and effective attraction.

C. Size Dependence. Another important experimental parameter is given by the variation of particle size. When microgels of different sizes between 6 and 70 nm

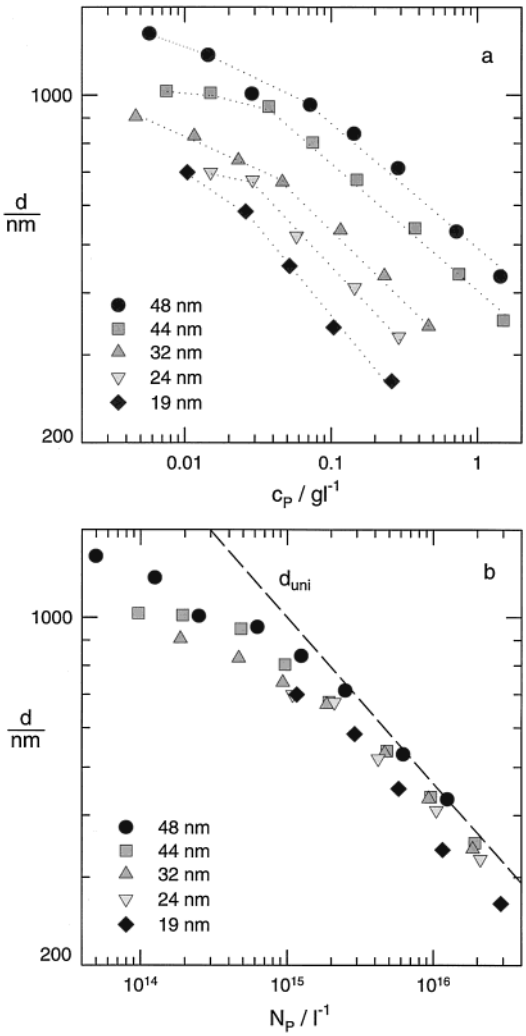

Figure 7. Interparticle distance d_{exp} obtained from the peak position in $S(q)$ for polyelectrolyte microgels with different sizes in salt-free solution: (a) as a function of the polymer mass concentration c_P and (b) as a function of the particle number density (particles per volume solution) N_P. Particle sizes r_H(NaCl) are given in the figure.

are examined, the described phase behavior, i.e., phase separation below a certain concentration, is found for all samples.

Figure 7a displays the interparticle distance data as a function of polymer mass concentration for microgels of different sizes. Numerical data are given in Table 3. In the case of the smallest microgel with $r_H = 6.7$ nm the polymer-rich phase does not sediment, but small domains of stronger scattering intensity are found within the less scattering phase. Therefore, it is not possible to measure the pure phases separately in this case. On the other hand, particles were examined only up to a size where multiple scattering effects can be definitely excluded.

A more direct comparison is enabled when plotting the corresponding distance data as a function of the particle number density, i.e., number of particles per volume solution, as shown in Figure 7b. Again, for ideal solutions with uniform distributed particles one would expect all data points lying on one line with the slope $^1/_3$. The figure demonstrates that the distances are smaller and the scaling exponents lower for all investigated particle sizes. Thus, the basic observation of "electrostatic attraction" is made for the whole examined range of colloid size from 6 nm $< R <$ 70 nm.

Table 3. Solution Parameters and Interparticle Distance Data for Concentration-Dependent Experiments on Polyelectrolyte Microgels with Different Sizes: K24 with r_H(NaCl) = 44 nm, K28 with r_H(NaCl) = 37 nm, K33 with r_H(NaCl) = 24 nm, and K35b with r_H(NaCl) = 19 nm[a]

sample	c_P/(g/L)	N_P/L^{-1}	ϕ	d_{exp}/ nm	d_{uni}/ nm
K24	1.500	1.93×10^{16}	6.65×10^{-3}	351.5	372.8
	0.750	9.65×10^{15}	3.33×10^{-3}	435.5	469.7
	0.375	4.83×10^{15}	1.66×10^{-3}	538.9	591.8
	0.150	1.93×10^{15}	6.65×10^{-4}	675.0	803.2
	0.075	9.65×10^{14}	3.33×10^{-4}	802.9	1011.9
	0.038	4.83×10^{14}	1.66×10^{-4}	947.6	1274.9
	0.015	1.93×10^{14}	6.65×10^{-5}	1010.2	1730.4
	7.5×10^{-3}	9.65×10^{13}	3.33×10^{-5}	1019.2	2180.1
K28	0.464	1.86×10^{16}	2.14×10^{-3}	342.0	377.2
	0.232	9.31×10^{15}	1.07×10^{-3}	432.3	475.3
	0.116	4.66×10^{15}	5.35×10^{-4}	534.0	598.8
	0.046	1.86×10^{15}	2.14×10^{-4}	668.7	812.7
	0.023	9.31×10^{14}	1.07×10^{-4}	739.7	1024.0
	0.012	4.66×10^{14}	5.35×10^{-5}	827.9	1290.1
	4.64×10^{-3}	1.86×10^{14}	2.14×10^{-5}	905.3	1751.0
K33	0.290	2.10×10^{16}	1.17×10^{-3}	326.0	362.2
	0.145	1.05×10^{16}	5.87×10^{-4}	409.3	456.4
	0.058	4.21×10^{15}	2.35×10^{-4}	519.9	619.4
	0.029	2.10×10^{15}	1.17×10^{-4}	675.0	780.4
	0.015	1.09×10^{15}	6.07×10^{-5}	699.6	972.2
K35b	0.260	2.90×10^{16}	9.43×10^{-4}	265.3	325.5
	0.104	1.16×10^{16}	3.77×10^{-4}	340.5	441.8
	0.052	5.80×10^{15}	1.89×10^{-4}	452.7	556.6
	0.026	2.90×10^{15}	9.43×10^{-5}	583.0	701.3
	0.0104	1.16×10^{15}	3.77×10^{-5}	699.6	951.8

[a] Data given are the same parameters as in Table 2.

Table 4. Scaling of Interparticle Distance with Concentration for Polyelectrolyte Microgels of Different Size in Salt-Free Solution

sample	r_H/nm (NaCl)	scaling exponent	sample	r_H/nm (NaCl)	scaling exponent
K8	48.0	0.25	K33	23.7	0.31
K24	43.5	0.28	K35b	19.8	0.33
K28	31.5	0.30			

The exact quantitative behavior is characteristically size dependent. With decreasing particle size, the difference between experimental interparticle distance and the calculated uniform interparticle distance increases; i.e., the particles get more attracted and become "less ideal" with decreasing size. In contrast, the slope of the interparticle distance with concentration increases with decreasing particle size, as given in Table 4, from a value of 0.25 for the 48 nm sample to a value of 0.33 for the 19 nm sample. Two possible mechanisms consistent with these experimental results that depend on particle size will be suggested in section F.

Furthermore, it is interesting to consider the data of the phase-separated solutions as a function of the concentration of the polymer-rich phase itself (instead of the initial polymer concentration as in Figure 7), which can be estimated from the scattering intensity. For this purpose, all scattering curves $I(q)$ are divided by the form factor $P(q)$, resulting in an "intensity-conserving" structure factor $bS(q)$, i.e., the structure factor times a concentration-dependent constant, as shown in Figure 8a. Thereby, for scattering curves with the measured q range larger than the extent of structuring, $bS(q)$ becomes constant at high q and the relative intensity value at large q is a quantitative measure of concentration. Data for higher concentration samples with a less extended q range relative to the structuring have to be extrapolated. Because of the congruence of the scattering curves after normalization,

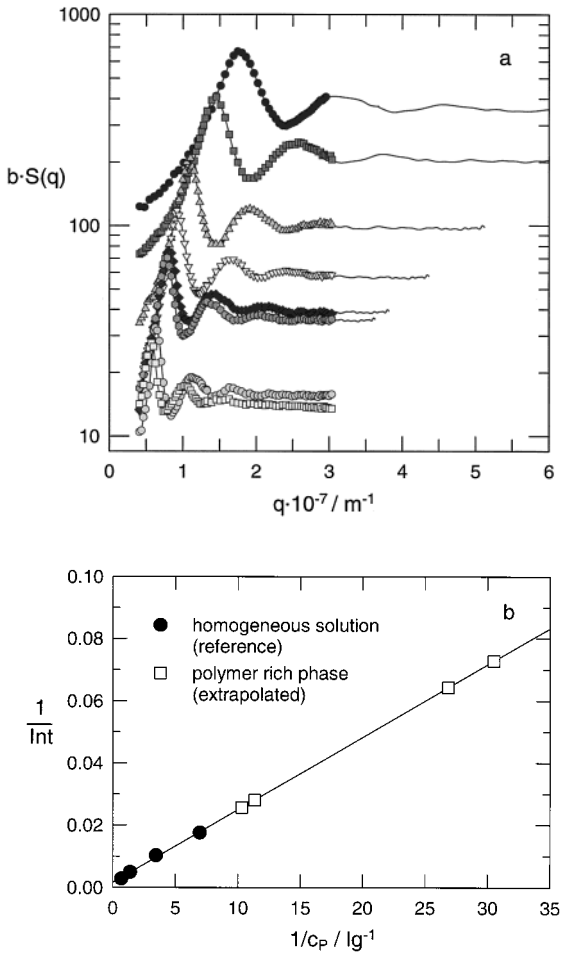

Figure 8. (a) Extrapolated "intensity-conserving" structure factors $bS(q)$ for scattering curves in Figure 1 (symbols see there). Higher concentration data are numerically extrapolated using a low-concentration scattering curve (full lines). (b) Determination of the polymer-rich phase concentration using the intensities obtained from (a).

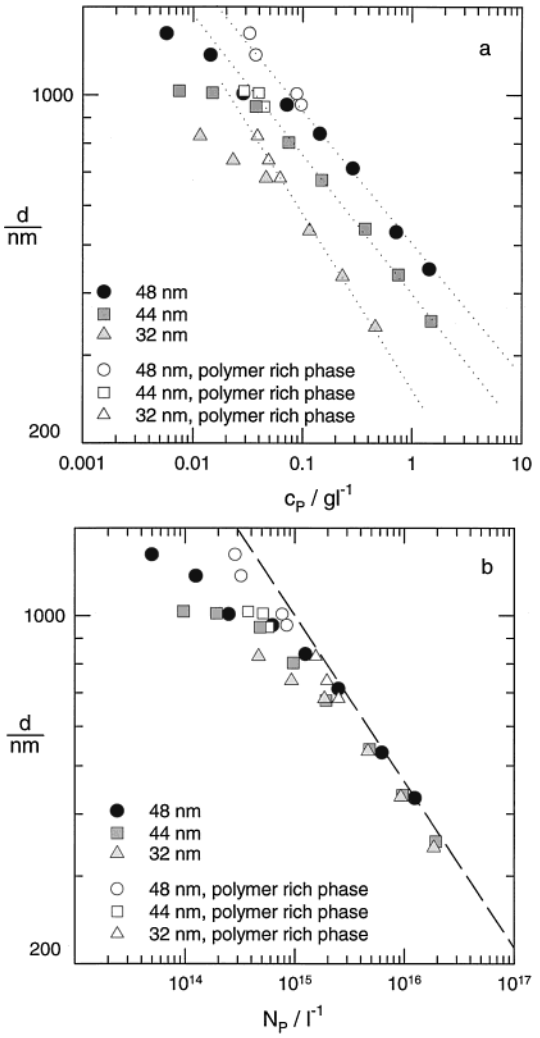

Figure 9. Interparticle distance data for microgels of differing size. Filled symbols correspond to macroscopically homogeneous solutions; open symbols represent data for the polymer-rich phase of the separated samples, plotted versus the concentration of this phase itself. (a) As a function of the polymer mass concentration c_P and (b) as a function of the particle number density (particles per volume solution) N_P.

this extrapolation can be numerically performed by using a low-concentration scattering curve. Results are shown in Figure 8a as full lines. Thus, a relative scattering intensity as measure of concentration is determined for all samples. We then create a calibration curve based on the homogeneous samples by fitting those data points with a $1/I = k_1/c_p + k_2$ relationship (according to the nonideality of the systems). This calibration curve can then be used for determination of the approximate concentration of the phase-separated samples, as shown in Figure 8b. In Figure 9, resulting interparticle distance dependencies, including data of phase-separated samples as a function of the estimated concentration of the polymer-rich phase (open symbols), are shown for three representative samples. The data points turn out to form the extrapolation of the homogeneous-solution data points (full symbols).

Interestingly, all data points for the homogeneous solutions, as well as the extrapolated data for the polymer-rich phases, appear to lie on a master curve when plotting the interparticle distance minus the particle diameter ($d - 2R$) as a function of the particle number density, as seen in Figure 10. The master curve has a slope of $^1/_3$ and again indicates the smaller-than-ideal interparticle distances. It is seen from this master plot that the value of $d - 2R$, which is the average distance between the particle surfaces, represents the relevant length scale governing the effective interaction potentials.

It is interesting to note that Belloni by a charge regulation model and the hypernetted chain integral equation theoretically derived an attractive potential between similarly charged colloids where exactly this surface−surface distance is the relevant length scale.[25] A quantitative comparison with the Belloni approach is however not possible for these macroscopically or microscopically phase-separated samples, since the Belloni approach does not have any solutions in these regimes. But the accordance of the significant parameters in our experiment and that theory encourages to consider the mechanisms of attraction discussed by Belloni.

More importantly at this point, the experimentally observed size dependence of the absolute contraction length and the scaling exponent explains partly why contrary experimental results are found in the literature. From the data shown in Figures 7, 9, and 10 one can see that both are a continuous function of particle size.

D. Influence of Added Salt. When studying the nature of electrostatic interaction forces, the role of ionic

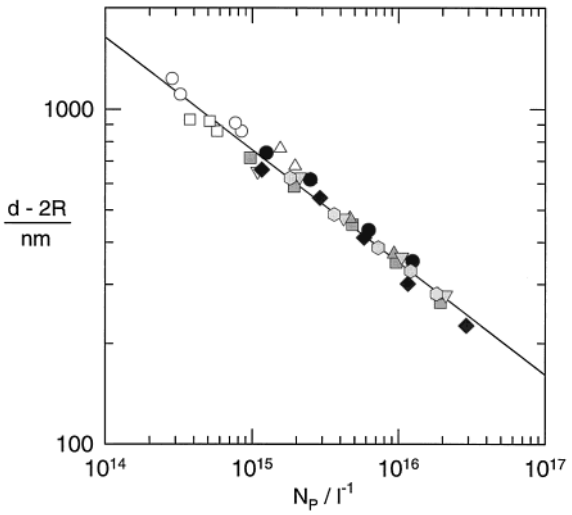

Figure 10. Interparticle distance minus particle diameter ($d - 2R$) as a function of the particle number density (particles per volume solution) N_p for polyelectrolyte microgels with different sizes in salt-free solution. Filled symbols correspond to macroscopically homogeneous solutions; open symbols represent data for the polymer-rich phase of the separated samples, plotted versus the concentration of this phase itself. Symbols are the same as given in the legend of Figure 7.

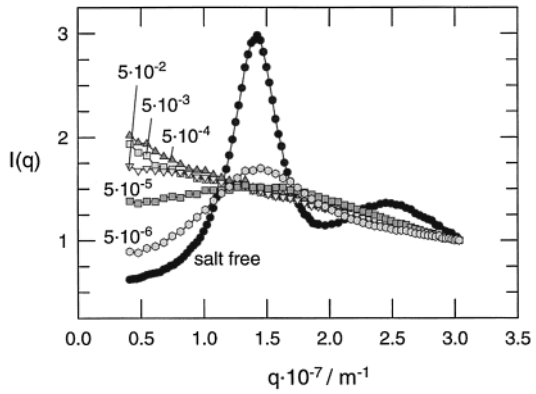

Figure 11. Scattering curves for a polyelectrolyte microgel with $r_H = 43.5$ nm in dependence of the salt concentration for a polymer concentration of 0.375 g/L. The salt concentrations given in the plot are in mol/L.

impurities or salt added by purpose is a relevant experimental question. Experiments with varying the salt content are carried out for two different polymer concentrations, 0.375 and 3.75×10^{-2} g/L, in the salt-free case the higher concentration corresponding to a homogeneous solution and the lower one corresponding to a phase-separated state. The NaCl concentration was varied between 5×10^{-6} and 0.5 mol/L.

None of the investigated salt-containing solutions phase-separates macroscopically. Even the solution with an added salt concentration of 5×10^{-6} mol/L stays homogeneous, in contrast to the "salt-free" solution with the same polymer concentration. In Figure 11 the scattering curves for the polymer concentration of 0.375 g/L are shown. In contrast to the pronounced structuration seen in the scattering curve of the salt-free solution, a NaCl concentration of 5×10^{-6} mol/L already reveals only one, very broad peak. At an added salt concentration of 5×10^{-4} mol/L no peak is detected at all.

The structuring of the macroions in solution obviously disappears very rapidly with added salt; i.e., already weak screening removes the structure causing force, underlining the electrostatic origin of both the structure formation and the attraction. On the other hand, this experimental set is a very good indication for the purity of the original "salt-free" samples and the quality of the established experimental procedures.

Further, it is worth mentioning that the disappearance of the structure peak between 5×10^{-5} and 5×10^{-4} mol/L added salt concentration corresponds to the transition $\kappa R < 1$ to $\kappa R > 1$, which relates to a change in the degree of structuring at $\kappa R \approx 1.3$ reported by Matsouka for salt-dependent experiments of classical latex spheres.[45−47]

E. Influence of the Particle Cross-Linking Density. A parameter of the microgel model system that is not offered by compact colloidal systems is the degree of particle cross-linking, i.e., the compactness of the particle structure. Indeed, a number of changes is observed when polyelectrolyte microgels of the same size but with different cross-linking densities are compared. In contrast to the 1/20 cross-linked microgel, no phase separation is observed at any concentration for the 1/40 and 1/80 cross-linked microgels. Figure 12 shows scattering curves for microgels with cross-linking densities 1/20, 1/40, and 1/80, i.e., increasingly loose structure. The loss of structure when changing the cross-linking density from 1/20 to 1/40 is remarkable. Only very broad peaks are found for the 1/40 microgel, whereas no peaks at all can be detected for the 1/80 microgel. Both microgels show an upturn in the scattering intensity at small angles.

By comparing the absolute scattering intensities (normalized values are plotted in Figure 12) as well as by ultracentrifugation experiments, the presence of compact aggregates as a reason for the increasing intensity at low angles can be excluded.

One possible reason for the upturn are domains of enhanced particle density, inside of which the particles are attracted, but still apart from each other. The interparticle distance within these domains is given by the position of the (broad) maximum in the case of the 1/40 sample. Small holes in a solution of structured particles would also cause a similar intensity increase at small angles. However, a microheterogeneity (of whatever kind) seems to be the most reasonable explanation in agreement with the experimental results. Thus, the picture of a two-state structure of particle-dense ordered regions and voids remains valid also for the less cross-linked samples. These regions however seem to be smaller for the less densely cross-linked sample; i.e., the size of the structured regions and the voids is now comparable to the length scale being connected with the q range window of static light scattering.

These trends can be related to the cross-linking density dependence that was found during examination of the viscometric behavior of these systems.[39] Viscometry showed that the electrostatic interaction potentials are significantly stronger for the less cross-linked samples; i.e., it is not the weakening of electrostatics which causes the structure to be less pronounced. Thus, it is our interpretation that the higher flexibility, shape fluctuation, and a beginning anisometry expected for the samples with lower cross-linking density enter the prefactors of the electrostatic repulsion and the electrostatic attraction terms in a different fashion (as it would be if attraction would be a multipole effect which

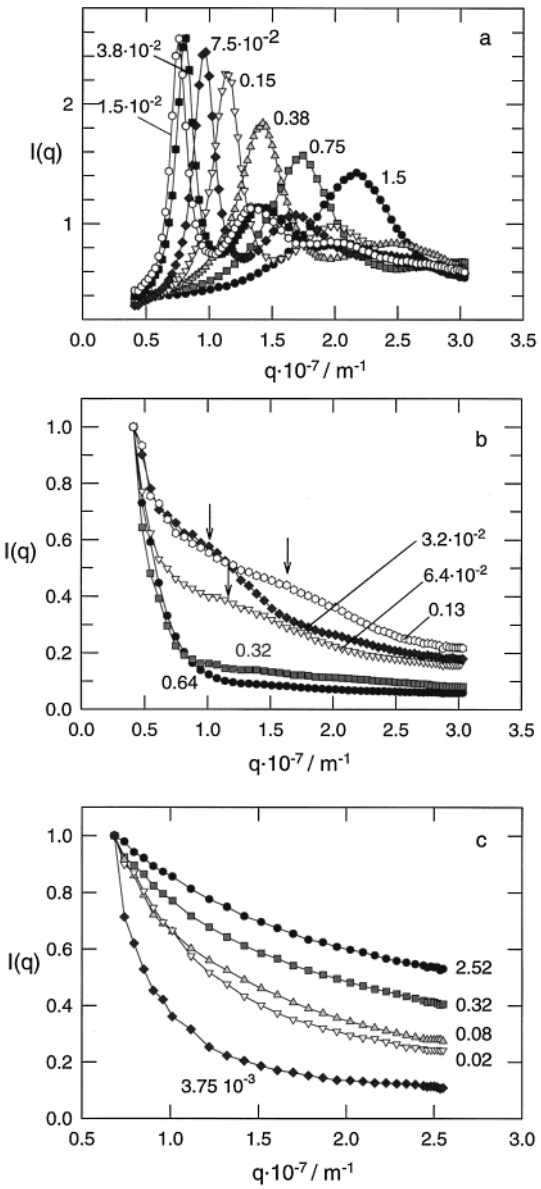

Figure 12. Scattering curves for three polyelectrolyte microgels with $r_H = 40$ nm and different cross-linking densities: (a) 1/20, (b) 1/40, and (c)1/80. The polymer concentrations are given in the plot in g/L.

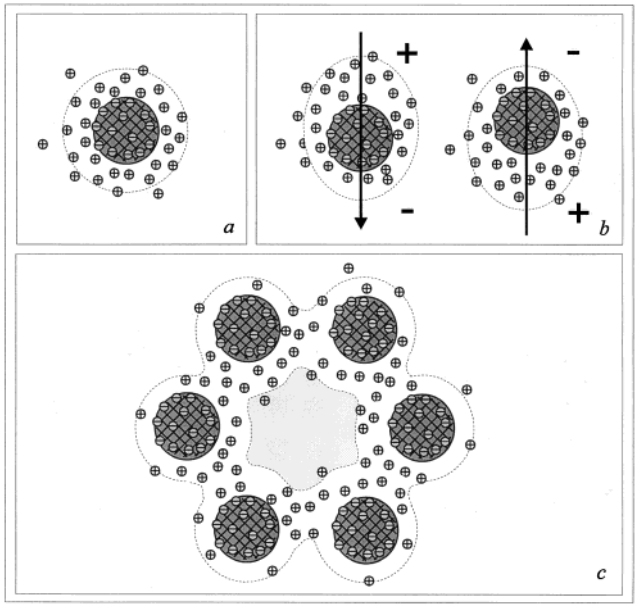

Figure 13. Qualitative models for possible interparticle electrostatic attraction in charged colloidal systems: (a) Negatively charged microgel with positively charged counterions distributed in a static spherical ionic sphere as predicted by linearized Poisson−Boltzmann approach (no attraction). (b) "*Fluctuation model*": fluctuation of the counterions results in attraction because of the formation of temporary dipoles. (c) "Colloidal orbital approach": the equilibrium counterion distribution is not spherical, but the counterion density between two or more macroions is enhanced resulting in an effective attraction between the macroions. (Note that in fact interparticle distances are much larger than particle dimensions in our system.)

can be dynamically averaged out) and prevent the loosely cross-linked microgels from the formation of structures with long-range order.

In this context it is interesting to note that a similar combination of low-q upturn and broad structure factor maximum is also found for linear polyelectrolytes and has recently been discussed by Amis et al. as "presence of supramolecular structures".[61] The upturn is further found for a number of different systems and has currently been analyzed for DNA solutions.[62] The formation of "correlated structures" has been intensively discussed in the context of "slow modes" in dynamic light scattering experiments on polyelectrolytes,[1,2] which will be applied on our microgel model system in a forthcoming paper.

F. Discussion of the Attraction. The coexistence of a condensed phase with a more diluted "gas phase" can only be explained by the presence of long-range attractive forces. The origin of these cannot be the classical Hamaker interaction, the range of which is only a few nanometers for colloids of the size investigated here, while interparticle distances lie between 200 and 2000 nm. Also, the salt dependence would be opposite to the one observed when caused by classical van der Waals forces. Further, interactions between hydrophobic parts are not expected to be of any importance, since polyelectrolyte microgels were designed to exclude such interactions. Hard-core depletion forces can also be excluded in these diluted systems with volume fractions between 1×10^{-5} and 1×10^{-2}.

Therefore, attractive forces arising from electrostatic effects have to be regarded. This involves consideration of effective multibody interactions between the colloidal particles as well as between the counterions. Because of the extensive discussions about the "electrostatic attraction", it seems useful to present a qualitative picture of our point of view here. Mainly two effects, which are not included in the classical linearized Poisson−Boltzmann approach, can be suggested, herein called the "*fluctuation model*" and the "*colloidal orbital approach*". Both are schematically shown in Figure 13.

The "fluctuation model" is based on the fact that the system of a charged colloid and its counterion cloud is not static in itself. Even if the equilibrium distribution of the counterions is spherical and symmetrically centered around the microgel, fluctuations will cause the formation of temporary dipoles, which in turn induce dipoles in neighboring ion clouds, resulting in an attraction between the dipoles. This "fluctuation model" is similar to the "temporal aggregate model" by Schmitz et al.[63]

The attraction due to fluctuations in the ion cloud is formally analogous to the attraction due to fluctuations

in the electron clouds considered in the classical London potentials. Therefore, a force law similar to the attractive part of the DLVO potential should apply, rescaled to larger radii and involving larger dipoles: the polarizable unit is a colloid plus ion cloud instead of electrons in a molecule. Usually, in the Lifshitz theory only fluctuations in the optical range are regarded for the Hamaker constant calculation. The fluctuation polarizabilities on a slower time scale should also be taken into account and are even more important here. Therefore, a large "*polyelectrolyte Hamaker constant*" might be a possibility to explain an intercolloidal attraction on the scale of a few hundred nanometers. In addition to the dipole−dipole attraction of the "fluctuation model", higher multipole interactions will also play a role (all of them being attractive at larger distances).

The "colloidal orbital approach" refers to a second important contribution that is not considered from the linearized Poisson−Boltzmann/MSA point of view: the nonspherical counterion distribution in regularly packed colloids. As in the case of the H_2^+ molecule as an analogue, enhancing the density of counterions between two macroions results in an effective "binding" or attraction. This idea corresponds to a number of similar ideas in the literature, such as the one of Schmitz, who recently pointed out the importance of multibody clusters that are stabilized by shared electrolyte ions in a theoretical work on the "juxtaposition of potential fields".[37] Another close analogy has to be seen in the work of Belloni,[21,25,26] who suggested that ion adsorption (as well as degree of dissociation) depends on the local electric fields, which makes the charge distribution anisometric and results in an additive component of net attraction between the particles.

Both different classes of mechanisms are expected to contribute to the effective attraction between similarly charged macroions, and it is not straightforward to relate the observed phenomena to one of the two mechanisms.

4. Conclusions

Spherical polyelectrolyte microgels that do not undergo conformational shape changes have been employed as a "pure Coulombic" model system in order to analyze the static structure of polyelectrolyte solutions.

The aqueous salt-free solutions of all investigated samples with radii between 6 and 70 nm yield scattering profiles with well-pronounced peaks displaying the long-range particle ordering. Interparticle distances indicate a microheterogeneity of the solutions. Domains with long-range particle ordering coexist with a polymer-poor phase that can be a "void" or "gaslike" unstructured region. At low concentrations, the aqueous salt-free solutions macroscopically separate into two phases, the particle density in both phases differing by a factor of about 200.

The phase coexistence requires the existence of long-range attractive forces. Since our experiments are designed in a way that sedimentation, Hamaker attraction, and hard-core depletion forces can be excluded, this attractive interaction has to be electrostatic in nature.

The systematic investigation of macroions over a decade of radii in a mesoscopic size range covers for the first time the gap between common linear polyelectrolytes and classical latex spheres. A continuous change in the scaling exponent relating the interparticle distance to the mass concentration from 0.33 for the smallest ($R = 17$ nm) to 0.25 for the largest particles ($R = 48$ nm) investigated is found. The absolute deviations of measured and calculated interparticle distance are however maximal for the smaller particles; i.e., the smaller the particles, the more important is the relative contribution of the attraction term as compared to electrostatic repulsion.

The presence of microscopic domains and the electrostatic nature of the attractive force are further confirmed by cross-linking density and salt concentration dependent experiments.

Two qualitative pictures describing the situation are delineated the "*fluctuation model*", based on the formation of temporary dipoles by fluctuations in the counterion cloud, and the "*colloidal orbital approach*", based on an enhanced counterion density between two or more macroions (or a similarly shaped anisometry of the dissociation of the surface charges themselves). Both attraction mechanisms are not regarded in the classical DLVO theory, which however was not constructed to describe more complex interactions in coupled multiparticle situations.

Acknowledgment. The authors thank Heimo Schnablegger and Andreas Briel for extended discussions, Helmut Cölfen for the introduction into ultracentrifugation, and Erich C. for general support. The financial support of the Max-Planck Society is gratefully acknowledged.

References and Notes

(1) Schmitz, K. S. *Macroions in Solution and Colloidal Suspension*; Verlag Chemie: New York, 1993.
(2) Förster, S.; Schmidt, M. *Adv. Polym. Sci.* **1995**, *120*, 51.
(3) Langmuir, I. *J. Chem. Phys.* **1938**, *6*, 873.
(4) Kose, A.; Ozaki, M.; Takano, K.; Kobashi, K.; Hachisu, S. *J. Colloid Interface Sci.* **1973**, *44*, 330.
(5) Ise, N.; Okubo, T:, Sugimura, M.; Ito, K.; Nolte, H. J. *J. Chem. Phys.* **1983**, *78*, 536.
(6) Ise, N.; Ito, K.; Okubo, T.; Dosho, S.; Sogami, I. *J. Am. Chem. Soc.* **1985**, *107*, 8074.
(7) Ise, N.; Okubo, T.; Ito, K.; Dosho, S. *J. Colloid Interface Sci.* **1985**, *103*, 292.
(8) Ito, K.; Nakamura, H.; Ise, N. *J. Chem. Phys.* **1986**, *85*, 6143.
(9) Ito, K.; Ise, N. *J. Chem. Phys.* **1987**, *86*, 6502.
(10) Ito, K.; Okumura, H.; Yoshida, H.; Yoshihiro, U.; Ise, N. *Phys. Rev. B* **1988**, *38*, 852.
(11) Ito, K.; Yoshida, H.; Ise, N. *Science* **1994**, *263*, 66.
(12) Yoshida, H.; Ise, N.; Hashimoto, T. *Langmuir* **1995**, *11*, 2853.
(13) Kesavamoorthy, R.; Rajalakshimi, M.; Rao, C. B. *J. Phys.: Condens. Matter* **1989**, *1*, 7149.
(14) Sogami, I.; Ise, N. *J. Chem Phys.* **1984**, *81*, 6320.
(15) Woodward, C. E. *J. Chem Phys.* **1988**, *89*, 5140.
(16) Overbeek, J. Th. G. *J. Chem Phys.* **1987**, *87*, 4406.
(17) Smalley, M. V. *Mol. Phys.* **1990**, *71*, 1251.
(18) Schmitz, K. S. *Langmuir* **1996**, *12*, 1407.
(19) Rouzina, I.; Bloomfield, V. A. *J. Phys. Chem.* **1996**, *100*, 9989.
(20) Patey, G. N. *Ber. Bunsen-Ges. Phys. Chem.* **1996**, *100*, 885.
(21) Belloni, L.; Spalla, O. *Ber. Bunsen-Ges. Phys. Chem.* **1996**, *100*, 905.
(22) Roij, R.; Hansen, J. P. *Phys. Rev. Lett.* **1997**, *79*, 2082.
(23) Gronbach-Jensen, N.; Mashl, R. J.; Bruinsma, R. F.; Gelbart, W. M. *Phys. Rev. Lett.* **1997**, *78*, 2477.
(24) Hribar, B.; Vlachy, V. *J. Phys. Chem.* **1997**, *101*, 3457.
(25) Belloni, L.; Spalla, O. *J. Chem. Phys.* **1997**, *107*, 465.
(26) Belloni, L. *Colloids Surf. A* **1998**, *140*, 227.
(27) Ito, K.; Yoshida, H.; Ise, N. *Chem Lett.* **1992**, 2081.
(28) Ito, K.; Yoshida, H.; Ise, N. *Science* **1994**, *263*, 66.
(29) Ito, K.; Kuramoto, K.; Kitano, H. *J. Am. Chem. Soc.* **1995**, *117*, 5005.
(30) Crocker, J. C.; Grier, D. G. *Phys. Rev. Lett.* **1996**, *77*, 1897.
(31) Larsen, A. E.; Grier, D. G. *Phys. Rev. Lett.* **1996**, *76*, 3862.
(32) Larsen, A. E.; Grier, D. G. *Nature* **1997**, *230*, 385.
(33) Okubo, T. *J. Chem. Phys.* **1987**, *86*, 2394, 5182.
(34) Okubo, T. *Colloid Polym. Sci.* **1987**, *265*, 598.

(35) Okubo, T. *J. Chem. Phys.* **1988**, *88*, 2038, 5182, 6581.
(36) Okubo, T. *Colloid Polym. Sci.* **1988**, *266*, 1042, 1049.
(37) Schmitz, K. S. *Langmuir* **1997**, *13*, 5849.
(38) Antonietti, M.; Bremser, W.; Müschenborn, D.; Rosenauer, C.; Schupp, B.; Schmidt, M. *Macromolecules* **1991**, *24*, 6636.
(39) Antonietti, M.; Briel, A.; Förster, S. *J. Chem. Phys.* **1996**, *105*, 7795.
(40) Antonietti, M.; Basten, R.; Lohmann, S. *Macromol. Chem. Phys.* **1995**, *196*, 441.
(41) Antonietti, M.; Hentze, H. P. *Adv. Mater.* **1996**, *8*, 840.
(42) Schnablegger, H.; Glatter, O. *Appl. Opt.* **1991**, *30*, 4889.
(43) Schnablegger, H.; Glatter, O. *J. Colloid Interface Sci.* **1993**, *145*, 228.
(44) The observed difference is larger than any difference that can occur because of different geometry assumptions. Anyway, by plotting the values for a cubic lattice, we stay on the "conservative" side: For random distribution the experimental distance would be even smaller, i.e., the difference to the calculated value even larger. Also note that the scaling behavior is independent of any geometry assumptions.
(45) Matsuoka, H.; Harada, T.; Yamaoka, H. *Langmuir* **1994**, *10*, 4423.
(46) Matsuoka, H.; Harada, T.; Kago, K.; Yamaoka, H. *Langmuir* **1996**, *12*, 5588.
(47) Harada, T.; Matsuoka, H.; Ikeda, T.; Yamaoka, H. *Langmuir* **1999**, *15*, 573.
(48) Blum, L. *Mol. Phys.* **1975**, *30*, 1529.
(49) Blum, L.; Hoye, J. S. *J. Chem. Phys.* **1977**, *77*, 1428.
(50) Blum, L.; Hoye, J. S. *J. Phys. Chem.* **1977**, *81*, 1311.
(51) Nägele, G.; Klein, R.; Medina-Noyola, M. *J. Chem. Phys.* **1985**, *83*, 2560.
(52) Chu, X.; Wasan, T. *J. Colloid Interface Sci.* **1996**, *184*, 268.
(53) Salgi, P.; Guerrin, J. F.; Rajagopalan, R. *Colloid Polym. Sci.* **1992**, *270*, 785.
(54) Salgi, P.; Ragajopalan, R. *Adv. Colloid Interface Sci.* **1993**, *43*, 169.
(55) Härtl, W.; Versmold, H. *Mol. Phys.* **1983**, *50*, 815.
(56) Härtl, W.; Versmold, H.; Wittig, U. *Ber. Bunsen-Ges. Phys. Chem.* **1984**, *88*, 1063.
(57) Härtl, W.; Versmold, H. *J. Chem Phys.* **1988**, *88*, 7157.
(58) Versmold, H.; Wittig, U.; Härtl, W. *J. Chem Phys.* **1991**, *95*, 9937.
(59) Härtl, W.; Versmold, H.; Zhang-Heider, X. *Ber. Bunsen-Ges. Phys. Chem.* **1991**, *95*, 1105.
(60) Wagner, N. J.; Krause; R.; Rennie, A. R.; Daguanno, B.; Goodwin, J. *J. Chem. Phys.* **1991**, *95*, 494.
(61) Ermi, B. D.; Amis, E. J. *Macromolecules* **1997**, *30*, 6937.
(62) Borsali, R.; Nguygen, H.; Pecora, R. *Macromolecules* **1998**, *31*, 1548.
(63) Schmitz, K. S.; Lu, M.; Singh, N.; Ramsey, D. J. *Biopolymers* **1984**, *23*, 1637.

MA000235V